RUNNING TITLE: Scaling photosynthesis from gene to leaf

TITLE: Combining gene network, metabolic, and leaf-level models show means to future-proof soybean photosynthesis under rising CO_2.

Kavya Kannan[1*], Yu Wang[2*], Meagan Lang[3], Ghana S. Challa[4], Stephen P. Long[1,2,3,4,5,6], Amy Marshall-Colon[1,2,3,4]

[1]Department of Plant Biology, University of Illinois Urbana Champaign, USA

[2] The Carl R. Woese Institute for Genomic Biology, University of Illinois Urbana-Champaign, USA

[3]National Center for Supercomputing Applications at the University of Illinois Urbana-Champaign, USA

[4]Institute for Sustainability, Energy, and Environment, University of Illinois Urbana-Champaign, USA

[5]Department of Crop Sciences, University of Illinois Urbana Champaign, USA

[6]Lancaster Environment Centre, Lancaster University, Lancaster University, Lancaster, LA1 4YQ, UK

*These authors contributed equally to this work.

ABSTRACT

Global population increase coupled with rising urbanization underlies the predicted need for 60% more food by 2050, but produced on the same amount of land as today. Improving photosynthetic efficiency is a largely untapped approach to addressing this problem. Here, we scale modeling processes from gene expression through photosynthetic metabolism to predict leaf physiology in evaluating acclimation of photosynthesis to rising [CO_2]. Model integration with the yggdrasil interface enabled asynchronous message passing between models. The multiscale model of soybean photosynthesis calibrated to physiological measures at ambient [CO_2] successfully predicted the acclimatory changes in the photosynthetic apparatus that were observed at 550 ppm [CO_2] in the field. We hypothesized that genetic alteration is

necessary to achieve optimal photosynthetic efficiency under global change. Flux control analysis in the metabolic system under elevated [CO_2] identified enzymes requiring the greatest change to adapt optimally to the new conditions. This predicted that Rubisco was less limiting under elevated [CO_2] and should be down-regulated allowing re-allocation of resource to enzymes controlling the rate of regeneration of ribulose-1:5 bisphosphate (RubP). By linking the GRN through protein concentration to the metabolic model it was possible to identify transcription factors (TF) that matched the up- and down-regulation of genes needed to improve photosynthesis. Most striking was TF GmGATA2, which down-regulated genes for Rubisco synthesis while up-regulating key genes controlling RubP regeneration and starch synthesis. The changes predicted for this TF most closely matched the physiological ideotype that the modeling predicted as optimal for the future elevated [CO_2] world.

KEYWORDS: Gene network model, metabolic model, photosynthesis, global change, Soybean, transcription factors, multiscale modeling, model integration

INTRODUCTION

As the world's most important seed legume and most widely grown dicotyledonous crop, the future-proofing of photosynthesis in soybean (*Glycine max* (L.) Merr.) under rising atmospheric concentrations of CO_2 ($[CO_2]$) is of importance. Down-regulation of light-saturated net leaf CO_2 uptake (A_{sat}) at elevated $[CO_2]$ has been reported for many C_3 crops, yet the mechanism underlying this response is poorly understood. Under current $[CO_2]$, A_{sat} in C_3 crops is most commonly limited by the *in vivo* Rubsico activity ($V_{c,max}$) (Long et al., 2004). However, as $[CO_2]$ continues to rise, it follows from the steady-state biochemical model of photosynthesis of (Farquhar et al., 1980) and its subsequent modifications (Von Caemmerer, 2000) that control will shift from Rubisco to RubP regeneration (Long et al., 2004), which is represented by the maximum *in vivo* rate of whole chain electron transport (J_{max}). While described by electron transport, most evidence now points to this being limited by the metabolic steps of carbon metabolism leading to RubP regeneration (Raines, 2003, Stitt and Sonnewald, 1995). This shift from Rubisco- to RubP- limited photosynthesis permits a reduction in leaf Rubisco content without a loss in A_{sat} (Woodrow, 1994, Long et al., 2004, Ainsworth and Long, 2005). Because Rubisco accounts for the largest single share of leaf N, optimization of Rubisco content would maximize the efficiency of use of this commonly limiting resource (Drake et al., 1997, Long et al., 2004).

When $[CO_2]$ is increased around a photosynthesizing leaf, A_{sat} can increase for two reasons, first the K_M of Rubisco for CO_2 is close to the current atmospheric concentration, so elevated $[CO_2]$ increases the velocity of carboxylation, and secondly, CO_2 competitively inhibits the oxygenation reaction that produces phospho-glycolate and in turn photorespiration. This latter effect is particularly important because it increases the efficiency of net CO_2 uptake by diverting ATP and NADPH (generated by the light reactions) away from photorespiratory metabolism to photosynthetic assimilation, and so will increase A_{sat} regardless of other limiting factors. Under rising $[CO_2]$ both factors will increase A_{sat} when $V_{c,max}$ is limiting, but only the second factor when J_{max} is limiting. Assuming the average specificity and K_M for CO_2 and O_2 for Rubisco from terrestrial plants, and a constant intercellular versus external $[CO_2]$, one can calculate the increase in A_{sat} that would result from an increase in atmospheric $[CO_2]$. Following the procedure of (Long et al., 2004) for a leaf temperature of 25 °C, the increase in atmospheric $[CO_2]$ from today's 400 µmol mol^{-1} to 550 µmol mol^{-1} would increase Rubisco-limited and

RubP-limited photosynthesis by 31% and 9%, respectively. 550 µmol mol^{-1} is the concentration forecast for 2050 assuming current emissions trends continue (RCP8.5, (Pachauri et al., 2014)). At current atmospheric [CO_2] soybean leaf photosynthesis is at the transition point between $V_{c,max}$- and J_{max}-limitation (Bernacchi et al., 2005). Therefore, as [CO_2] rises soybean photosynthesis would become RubP-limited. If however, resource currently invested in Rubisco was re-allocated to increased J_{max} then this transition point would move to a higher [CO_2] and a 31% rather than 9% increase in A_{sat} could be obtained, without any increased total investment of protein in the photosynthetic apparatus. When grown under elevated [CO_2] in open-air field conditions, is an increase in J_{max} observed at the expense of $V_{c,max}$?

In two consecutive years, (Bernacchi et al., 2005) analyzed photosynthesis in a modern highly productive soybean cultivar under open-air [CO_2] elevation using Free-Air Concentration Enrichment (FACE) (Long et al., 2006). Compared to control plants those grown in [CO_2] elevated to 550 µmol mol^{-1} showed a shift in control of A_{sat} from co-limitation of $V_{c,max}$ and J_{max} to limitation solely by RubP-limitation. There was a significant 5% decrease in the ratio of $V_{c,max}$:J_{max}, showing a decline in Rubisco activity relative to the capacity for RubP regeneration (Bernacchi et al., 2005). However, while acclimation had occurred it was insufficient to maximize the potential increase in A_{sat}, had the system responded to fully re-optimize investment of resources. At 25 °C, re-optimizing the system to 550 ppm was calculated to require a 35% reduction of investment in Rubisco and re-allocation of that protein to the apparatus for regeneration of RubP (Drake et al., 1997, Long et al., 2004), while only a 5% change was observed. The plant was apparently over-investing in Rubisco and under-investing in the apparatus determining regeneration of RubP. How might genetic manipulation be used to achieve re-optimization and prepare soybean and other crops to sustainably maximize photosynthetic efficiency and in turn crop productivity under future conditions?

Here we combine a metabolic model of C_3 photosynthetic metabolism, including the C_2 photorespiratory pathway, mathematically representing all discrete steps of photosynthesis from light and CO_2 absorption to starch and sucrose synthesis (Zhu et al., 2007, Zhu et al., 2013) with a gene network model to predict observed acclimatory changes. This is successfully tested against observed acclimatory changes of photosynthesis in soybean grown at elevated [CO_2]. Finally, via sensitivity analysis and dynamic gene regulatory network analysis, the combined

model is used to predict genetic changes, including expression levels of transcription factors, that could fully optimize leaf photosynthetic efficiency to future elevated [CO_2] conditions.

MULTISCALE MODEL DEVELOPMENT

To predict what genes may transcriptionally regulate the soybean response to elevated [CO_2], it was necessary to develop a mechanistically informed model in which the multi-scale response could be explored. We have previously developed complete mechanistic metabolic models of photosynthetic carbon metabolism that successfully predict dynamic responses of leaf chlorophyll fluorescence and fluxes of CO_2 and O_2 to changes in light, [CO_2] and [O_2] (Zhu et al., 2007, Zhu et al., 2013). While each of these models provided new insights about photosynthesis, when combined with optimization routines to predict optimal investments for different environments, they are not equipped to predict transcriptomic and genetic changes that could achieve those optimal patterns of investment. The generalization of whole plant metabolism and signaling pathways often results in simulations with low prediction accuracy upon model perturbation. Multiscale models that mimic the biological flow of information across scales have been shown to have higher prediction accuracy than models at individual scales, especially when simulating conditions different from the original training data (Chew et al., 2014). To our knowledge, no current model of photosynthesis in soybean scales from genes to organs. Such a model could potentially simulate system-wide changes in photosynthesis in response to targeted genetic perturbations.

To predict leaf-level responses of net CO_2 uptake, a metabolic model (e-Photosynthesis) was combined with a leaf micrometeorological model that integrated boundary layer conductance, stomatal conductance, and leaf energy balance (Drewry et al., 2010, Nikolov et al., 1995). Our prior e-Photosynthesis model (Zhu et al., 2013) simulates fluxes through some 70 reactions involved in the light and dark reactions of C_3 photosynthesis. The steady-state photosynthesis rate predicted by the e-Photosynthesis model replaced the leaf model prediction that was based on the Farquhar model of photosynthesis (Nikolov et al., 1995). Leaf temperature, light intensity and intercellular CO_2 concentration predicted by the leaf model were used as inputs for the e-Photosynthesis model. The integrated leaf metabolic and micrometeorological model effectively simulates the observed response to net leaf CO_2 uptake to [CO_2] observed for soybean in the field (Bernacchi et al., 2005) (Figure 1, Supplemental figure 1). However, it lacks

any capacity to predict the observed decrease in $V_{c,max}$ and increase in J_{max} that resulted from growth in elevated [CO_2]. This is because the model lacks any connection to the underlying changes in gene expression that may cause this altered photosynthetic phenotype.

The altered photosynthetic phenotype likely resulted from adjusted enzyme concentrations in soybean leaves grown under ambient and elevated CO_2 concentrations. Such CO_2-induced changes in protein concentrations was shown for total protein concentration in barley, rice, wheat, soybean, and potato (Taub et al., 2007) and for specific proteins via proteomic analysis in rice (Bokhari et al., 2007), wheat (Yousuf et al., 2017), and grape (Zhao et al., 2019). A decrease in the quantity of Rubisco is a pervading feature of plants grown in the field under elevated [CO_2] (Ainsworth and Long, 2005). However, the e-Photosynthesis model only allows substrate (CO_2) concentration to change, which results in altered reaction rates, but lacks capacity to predict acclimatory changes in enzyme concentrations. By including gene expression data from soybean plants grown under ambient and elevated [CO_2] (Leakey et al., 2009), it is possible to make predictions about changes in enzyme concentrations.

Gene expression data cannot be used as direct input for the e-Photosynthesis model, which can only accept enzyme concentrations. Also, transcriptome data from microarray or RNA-sequencing technologies provide relative and not absolute quantification of mRNA transcripts. To overcome these challenges and inform the e-Photosynthesis model with gene expression data, a model was needed to computationally translate mRNA to protein concentration. An ordinary differential equation (ODE) was adapted from (Becskei and Serrano, 2000), and given as: $(\boldsymbol{\Delta p} = \left(\frac{1}{1+\frac{p}{d}} \times \boldsymbol{L} \times \boldsymbol{r}\right) - (\boldsymbol{U} \times \boldsymbol{p}))$,

Eq. 1

where, L and U are the estimated gene family-specific protein synthesis and degradation rates (Li et al., 2017), respectively, r is the mRNA level, p is the initial protein concentration, and d is the upper limit of protein translation. It is assumed that r and p are equal (Edfors et al., 2016), and p is based on starting protein concentration estimates from the e-Photosynthesis model. To simulate steady-state protein concentrations in elevated CO_2, p was adjusted based on the proportion of change in mRNA level between ambient and elevated [CO_2] for a given gene.

The change in predicted, relative protein concentrations between ambient and elevated CO_2 conditions (ProteinRatio) was used to adjust the enzyme concentration and activity of each

gene involved in the light and dark reactions of photosynthesis represented in the e-Photosynthesis model, as follows:

$$V_{\max\_ele} = V_{\max\_0} \cdot [E.ProteinRatio] \quad \text{Eq 2}$$

where, V_{max_ele} is the maximum activity of each enzyme in elevated CO_2, V_{max_0} is the original maximum activity of each enzyme in ambient CO_2, and E is the estimated enzyme concentration.

Because the protein translation model and metabolic/leaf level models are implemented in different programing languages (Python and MATLAB) respectively, they cannot communicate with each other directly without significant alteration of the model code or through manual integration by running the model programs independently and using files to pass information between them. In order to integrate the models programmatically (Figure 2), we used the yggdrasil framework. yggdrasil is an open-source Python package developed by the Crops *in silico* research group for connecting models written in different programming languages through simple interfaces in the model's language of implementation. Based on information on the target models and connections between the models provided in human-readable specification files, yggdrasil runs the designated models in parallel and coordinates asynchronous communication between the models as they run. Asynchronous message passing allows models to continue working after sending output to the next model in the network without waiting for the output to be received, thereby improving the performance of the overall model integration as models can complete calculations simultaneously in separate processes. yggdrasil currently supports connecting models written in Python, Matlab, C and C++ on Linux, Mac OS, and Windows operating systems. Additional information on the yggdrasil package can be found in (Lang, 2019) or in the documentation (https://cropsinsilico.github.io/yggdrasil/).

METHODS

Differential Expression Analysis of Genes Responding to CO_2

The soybean transcriptome differential responses to growth in ambient and elevated [CO_2] was obtained previously using the Affymetrix *Glycine max* genechip (Leakey et al., 2009). These data were re-analyzed here to identify differentially expressed (DE) genes corresponding to leaf

tissue collected at the beginning of seed set when the canopy has attained full maturity. Probe sets were normalized using the GC Robust Multi-array Average (GCRMA) method. A one-way ANOVA was done in the R statistical software environment using the aov function of the stats package. The reanalysis identified 5005 DEGs on a statistical cutoff of P value <= 0.05 and Benjamini-Hochberg False Discover Rate (FDR) <= 0.3.

Construction of CO_2 responsive Gene Regulatory Network

Co-expression using mutual rank

Mutual rank analysis (Obayashi and Kinoshita, 2009) was used to obtain highly significant co-expression relationships among differentially expressed genes (DEGs). In mutual rank analysis, the Pearson Correlation Coefficient (PCC) is calculated between the gene of interest and all other DEGs, then sorted based on their PCC ranks, in which the gene pair having the highest correlation value is given rank 1 (Obayashi and Kinoshita, 2009). Mutual Rank is calculated from PCC rank by taking the geometric mean between PCC ranks from gene A to gene B and from gene B to gene A, as these can be different. The ranks are scaled between 0 to 1, where MR of 1 indicates the most significant coexpression interaction. All interactions having an MR >= |0.8| and a PCC >= |0.6| were selected for the coexpression network. Interactions having a significant correlation were further filtered to retain only those that had predicted binding interactions between the TF and target gene as described below.

Static Gene Regulatory Network construction and analysis

To analyze gene regulatory networks, a DNA pattern search algorithm was performed (PlantPAN, http://plantpan2.itps.ncku.edu.tw/) (Medina-Rivera et al., 2015) to identify the presence of known *Cis*-regulatory elements (CREs) in the promoter region of genes of interest. Known CREs were obtained from the transcription factor databases Transfac (Matys et al., 2006), JASPAR (Sandelin et al., 2004), CISBP (Weirauch et al., 2014), and PlantTFDB (Jin et al., 2013), and NewPLACE (Higo et al., 1999). The promoter region considered in this study was the sequence 1 Kb upstream of the predicted or experimentally verified Transcription Start Site (TSS) for every gene obtained from PlantProm (Shahmuradov et al., 2003). Promoter regions of target genes were analyzed for an enrichment of CREs for a particular TF family. For this analysis, the average number of binding sites for a CRE in the putative 1 Kb up-stream promoter region of all the genes present in Soybean Wm82.a1.v1 was calculated. If a target gene

promoter has a greater than average number of TF family-specific binding sites present in its promoter, then the CRE of interest is considered over-represented.

Dynamic Gene Regulatory Network Model Construction

A dynamic Gene Regulatory Network (GRN) model was built using a linear regression algorithm to infer relationships between a dependent variable (in this case the expression of the putative target gene) and one or more independent variables (or predictors; in this case TFs). The resulting linear model was used to predict the response variable based on the states of the dependent variables. The regression algorithm was run in R using the LM function (Team, 2013), which optimizes variables of the linear model using a least squares fit between the response and dependent variables on training data (Eq 1) (Bjorck, 1996).

For example:

$$mRNA\_Target = g0 + (W1 * mRNA_{TF1}) + (W2 * mRNA_{TF2}) + \cdots \quad \text{Eq 3}$$

where, g0, W1, W2 are least squares optimized parameters for the linear model. mRNA_TF1, mRNA_TF2, etc. are expression values of TFs predicted to regulated target genes of interest in the static GRN. Parameters were optimized using training data, which ultimately resulted in a weight (W_x) that corresponds to the level of influence that a TF exerts on a predicted target gene's expression. A linear model was generated for every gene in the static CO_2-responsive GRN, and used to simulate the expression of genes of interest in both ambient and elevated CO_2 environments. All linear model equations are listed in Supplemental Table 1.

The training data was obtained from seven soybean Affymetrix microarray transcriptome datasets (GSE8432, GSE23129, GSE26198, GSE29740, GSE29741, GSE35427, GSE44685). While these datasets were derived from a variety of experimental conditions, they were chosen because samples were taken from similar tissue and developmental stage as those in the CO_2-responsive dataset used to build the static GRN (Leakey et al., 2009). Expression data from all training sets were commonly normalized by GCRMA and quality control analysis was performed; samples with a high variation in their median expression level within replicates were removed from the analysis. A total of 213 samples were used to train the linear regression model. The CO_2-responsive dataset that is used to build the static GRN was used as a test dataset for the linear model, to predict expression of the target gene using the optimized weight associated with every TF.

Protein translation model

A protein translation model (PTM) adapted from (Becskei and Serrano, 2000) was used to predict steady-state protein concentrations based on relative mRNA transcript levels (See Eq. 1) The model parameter *p* (and thus *r*) is obtained from the initial protein concentration used in the e-Photosynthesis metabolic model under the control (ambient CO_2 = 380 ppm) condition. To predict initial protein concentration in elevated CO_2 conditions (550 ppm), *p* was adjusted using the relative fold change in mRNA transcript levels measured between ambient and elevated CO_2 conditions. As stated earlier, *L* and *U* are protein synthesis and degradation rates, respectively, and denotes the increase or decrease in protein abundance per hour (denoted as g/L/hour). Soybean gene-specific *L* and *U* rates were estimated based on the rates of their Arabidopsis orthologs taken from (Li et al., 2017). If ortholog information for a gene was not available, *L* and *U* were estimated by taking an average of *L* and *U* rates for all Arabidopsis genes involved in photosynthesis.

The PTM model simulations resulted in steady-state protein concentration ratios between ambient and elevated [CO_2] conditions for every gene. Optimized parameter '*d*' was obtained in a gene specific manner such that, the steady-state protein concentration ratio between the two conditions (elevated/ambient) remains constant for that gene after a particular threshold '*d*' (see Supplemental Table 2). This protein concentration ratio was then used as one of the inputs for the e-Photosynthesis model (described below) in order to account for changes in gene expression as a factor influencing the enzyme kinetics of proteins in the primary C metabolism machinery. The model assumes constant temperature and constant concentration of RNA polymerase (El Samad et al., 2005).

Metabolic photosynthesis model

The soybean photosynthesis metabolic flux (MF) model is based on the e-Photosynthesis model (Zhu et al., 2013) and implemented in MATLAB. The e-Photosynthesis model is a general C_3 photosynthesis model that includes each discrete process from light capture to carbohydrate synthesis, including photorespiratory C_2 metabolism. In the model, the rate of change of the concentration of each metabolite is represented by an ordinary differential equation (ODE):

$$\frac{dC}{dt} = V_p - V_u \qquad \text{Eq 4}$$

Where, [C] represents metabolite concentration; V_p is the total rate of reaction(s) that produces C, and V_u is the rate of consumption. Rate equations for each enzyme catalyzed reaction were developed based on standard Michaelis-Menten equations for enzyme kinetics, with kinetic parameters corresponding to a temperature of 25°C. Four enzymes, including Rubisco, did not satisfy the conditions needed to apply Michaelis-Menten kinetics, and equations for their catalysis were as in (Zhu et al., 2007). Initial protein concentration of enzymes in the MM kinetics equation were obtained from (Zhu et al., 2013) (Supplemental Table 3). $V_{c,max}$ and J_{max} of soybean grown under ambient and elevated [CO_2] in the field had been determined previously (Bernacchi et al., 2005). This was the same germplasm, site and treatments from which the transcriptional data, used in developing the GRN, was obtained. Here the $V_{c,max}$ and J_{max} obtained in ambient [CO_2] was used to calibrated the metabolic model, which on integration with the other models was then used to attempt to predict the observed changes in the $V_{c,max}$ and J_{max} observed with growth at elevated [CO_2]. Calibration was achieve by adjustinge amounts of Rubisco to match the $V_{c,max}$ described for soybean grown in ambient [CO_2]. All other protein amounts in the metabolic model, were elevated maintaining the proportion used in (Zhu et al., 2013), until a J_{max} was achieved that matched that observed by (Bernacchi et al., 2005). This required multiplying each by 1.2 over those used in (Zhu et al., 2013) (Supplemental table 3). The enzyme kinetic parameters of e-Photosynthesis are for 25°C. Leaf temperatures in the simulations used here slightly exceeded this. To deal with these slight, but variable, increases in temperature parameters were adjusted to the actual leaf temperature (T_i) using a Q_{10} function, as described previously (Woodrow and Berry, 1988).

$$k_i = k_{25} \cdot Q_{10}^{\frac{T_i - 25}{10}} \qquad \text{Eq 5}$$

The predicted enzyme protein concentration changes as a percentage of that in ambient [CO_2] were assumed in direct proportion to the changes of enzyme activities (V_{max}) in the metabolic model. For example, if the predicted sedoheptulose-1:5 bisphosphatase (SBPase) protein concentration was predicted to increase by 3% under elevated [CO_2], then SBPase activity ($V_{max\_Rubisco}$) was also increased by 3% in metabolic model.

Sensitivity analysis of each step in the metabolic model

Metabolic control analysis defines the quantitative link between the flux through a pathway and the activity of an enzyme in terms of the flux control coefficient (Fell, 1998). The maximum activity of each enzyme (V_{maxi}) was both increased and decreased by 1% individually in the model to calculate the new photosynthesis rate (A^+ and A^-) for the two CO_2 concentrations (350 ppm vs 550 ppm) to identify the enzymes that most influence the net photosynthetic rate. The flux control coefficient (CC) of each enzyme was calculated as:

$$CC = \frac{\partial A}{\partial V_{max\,i}} \frac{V_{max\,i}}{A} \approx \frac{A^+ - A^-}{0.02 \cdot A} \qquad \text{Eq 6}$$

Where A is the original net leaf CO_2 uptake rate, before the simulated change in activity of enzyme i ($\tilde{o}V_{\max\,i}$).

Leaf level photosynthesis model

At the leaf level, the metabolic model was integrated with leaf level models of stomatal physiology, and energy balance based on the method of (Nikolov et al., 1995). Here, stomatal conductance is a function of predicted net leaf CO_2 uptake rate, humidity, and [CO_2] after (Collatz et al., 1991). Leaf energy balance takes account of intercepted short and long wave radiation, radiative energy loss from the leaf, convection and latent heat loss in transpiration. However, these models are inter-dependent. For example, CO_2 uptake rate affects stomatal conductance, stomatal conductance affects leaf temperature and leaf temperature affects CO_2 uptake rate. Solving these circular connections is achieved iteratively. Iteration continues until change to obtain a numerical solution of stomata conductance, leaf temperature, boundary-layer conductance and photosynthesis rate until changes in all four are <0.1% between iterations. This model is also implemented in MATLAB. Equations and parameters are listed in supplemental information (Supplemental table 4).

RESULTS

338 **A multiscale model of soybean can mimic photosynthetic acclimation observed in FACE**
339 **experiments**

340 The integrated model predicted new steady-state enzyme concentrations for selected
341 reactions belonging to the dark reactions and starch synthesis in the e-Photosynthesis model in
342 response to growth of soybean leaves under elevated [CO_2]. The ratio of predicted steady-state
343 enzyme concentrations in elevated to ambient CO_2 is used as one of the inputs in the e-
344 Photosynthesis model (Supplemental Table 5). Though the magnitude of the change is small, the
345 predicted CO_2 response is consistent with the altered photosynthetic phenotype, as shown by the
346 improved fit to the measured response of A_{sat} to leaf intercellular [CO_2] and the values of $V_{c,max}$
347 and J_{max} calculated from this response (Bernacchi et al., 2005) (Figure 1). Including the gene
348 expression data, the V_{cmax} of the predicted CO_2 response curve decreases from 115 to 109 μmol
349 m^{-2} s^{-1}, and J_{max} of the predicted curve increase from 149 to 153 μmol m^{-2} s^{-1}. Simulations reveal
350 no significant change in leaf temperature, transpiration and stomatal conductance
351 (Supplementary Figure 1). Importantly, the fully integrated model was able to simulate the
352 change in photosynthetic rate due to the acclimation response observed in soybean plants grown
353 under elevated [CO_2] (Figure 1). The predicted A_{sat} in 550 ppm [CO_2] increased by 17.7%
354 compared to ambient. Predicted metabolite concentrations also changed dynamically with
355 elevation of [CO_2], for example RubP decreased, PGA, T3P and SBP increased, as would be
356 expected from an increased flux into these pools with accelerated carboxylation and decreased
357 oxygenation at Rubisco (Figure 3).
358
359 ***in silico* perturbations reveal potential mechanisms for the transcriptional regulation of**
360 **photosynthetic acclimation**
361 Genes with a functional role in the same biological pathway are often co-expressed and
362 sometimes co-regulated. The identification of common cis-regulatory elements in the promoters
363 of tightly co-expressed genes is a good proxy for co-regulation (Allocco et al., 2004). The
364 corresponding transcription factors that bind to these CREs are promising targets for the
365 manipulation of whole pathway expression. The re-engineering of photosynthesis is needed to
366 increase crop productivity in response to climate change (Zhu et al., 2010), such as overcoming
367 the limitations caused by photosynthetic acclimation at elevated atmospheric [CO_2]. With a fully
368 integrated model of photosynthesis it was then possible to simulate the field-level photosynthetic

response to genetic perturbations under both ambient (380 ppm) and elevated (550 ppm) [CO_2]. The ideotype for elevated [CO_2] is one in which Rubisco content is substantially decreased and controlling components of the apparatus for RubP regeneration substantially increased. This problem was approached by revisiting the individual models to identify gene targets that significantly contribute to deliver this metabolic ideotype.

Sensitivity of the system to individual steps within photosynthetic carbon metabolism

To determine which steps in the system exert the strongest control on A_{sat} in both ambient and elevated [CO_2], a sensitivity analysis was performed by varying each parameter +/- 1% (Table 1). Control coefficients (CCs) are calculated as the ratio of change in the amount of one enzyme divided by change in A_{sat}. If a 1% change in enzyme x results in a 1% change in A_{sat} CC = 1, the maximum possible, while if the change in A_{sat} is zero, then CC = 0, meaning that no control is exerted by that enzyme. The sum of all control coefficients should approximate to 1. Rubisco has the highest CC of all enzymes in ambient [CO_2], while SBPase has the highest control coefficient in elevated CO_2 (Table 1). Nine enzymes with the highest CCs overall (>0.01) were further evaluated for transcriptional regulation.

A CO_2–responsive gene regulatory network reveals co-regulated genes

A static gene regulatory network (GRN) of the nine enzymes with the highest CCs from the e-Photosynthesis model was constructed using transcriptome data from soybean grown under ambient and elevated [CO_2] (Leakey et al., 2009). Network nodes represent the genes that encode the nine enzymes involved in photosynthesis with the highest CC. Network edges represent regulatory interactions between TFs and putative, co-expressed target genes as determined by rank correlation of expression (MR >= 0.8 and PCC >= |0.6|) and the significant presence of CREs in the promoter of target genes for a corresponding TF gene. The static GRN was used to define the regulatory interactions that contribute to the expression of each target gene, in which each gene of interest (GOI) may have more than one TF protein regulating its expression. A linear regression modeling approach (Karlebach and Shamir, 2008) was used to determine the strength of influence, or weight (w), of each TF predicted to regulate a GOI. The resulting equations containing weighted TF-target interactions that enabled dynamic simulations with the GRN, where the expression of any TF in the network could be modified (up- or down-regulated) and result in a predicted change in expression of the target GOI (Figure 4).

The dynamic GRN (Figure 5) was explored to identify TFs that would simultaneously down-regulate carboxylation of Rubisco and up-regulate RubP regeneration and starch synthesis. Based on network topology, the top three candidate TFs are GmWRKY71 (Glyma.07G023300), a bHLH transcription factor (Glyma.18G115700), and GmGATA2 (Glyma.01G169400) (Supplemental Figure 2). *in silico* perturbations were performed for each candidate TF in which the TF expression was eliminated (knock-out) or overexpressed. Simulations within the dynamic GRN resulted in newly predicted expression levels of all genes targeted by the TF of interest (Figure 4).

The predicted change in mRNA expression provided input for the protein translation model that in turn predicted steady-state enzyme concentrations under elevated and ambient [CO_2] as described in the Model Development section. The ratio of steady-state protein levels were then fed into the fully integrated photosynthesis model to obtain predicted changes in photosynthesis rate. The *in silico* over-expression of GmWRKY71 and GmGATA2, and the knockout of the bHLH TF resulted in a predicted increase in photosynthetic rate under both ambient and elevated [CO_2]. A simultaneous *in silico* over-expression of GmWRKY71 and knock-out of bHLH TF increased the overall photosynthesis rate compared to wild type, but these failed to significantly lower Rubisco and release the resource that would be needed to elevate capacity for RubP regeneration without more resource investment (Figure 6A-C). The most promising TF candidate according to model simulations is the overexpression of GmGATA2, which results in the most dramatic change to both the down-regulation of carboxylation and up-regulation of RubP regeneration based on the simulated A/Ci curve (Figure 6D).

DISCUSSION

Multi-scale models have the potential to identify and add missing mechanistic details about system function and generate new hypotheses to prioritize targeted engineering efforts in plant science (Marshall-Colon et al., 2017, Millar et al., 2019). More than 4,000 mathematical plant models were published over the last decade. The majority of these models describe one biological scale or process and generalize the un-modeled spatio-temporal processes as a single output from a black box. Linking single-scale models will improve the comprehensive investigation of biological systems, resulting in explanatory models with higher prediction

accuracy than models limited to one biological scale. The ability to interrogate biology at many resolutions can reveal emergent system behaviors that cannot easily be measured (Walpole et al., 2013). Multiscale models that link genes to phenotypes can accelerate the directed development of crop ideotypes. Until now metabolic modeling has predicted ideotypes with maximal photosynthetic efficiency for given environmental conditions with respect to distribution of resources between photosynthetic proteins. Achieving the ideotype then depends on identifying individual genes that might be up- or down- regulated. The multi-scale model may now be used not only to predict the metabolic ideotype, but the gene expression changes at the network level needed to achieve this. In turn, this has led, as demonstrated here, to the identification of transcription factors that can achieve the multiple gene expression changes needed by alteration of the expression of just one or two transcription factors.

In this study, we constructed a multiscale model of soybean leaf photosynthesis by integrating three models across molecular and organ-level scales using asynchronous message passing. By informing the leaf micrometeorological model with gene-level data, we were able to simulate the field-observed phenomena of photosynthetic acclimation in soybean plants grown under two different atmospheric CO_2 concentrations. Acclimation was previously suggested to be a transcriptionally driven process that increases the capacity of respiration (Leakey et al., 2009). This though does not explain the observed decrease in in vivo Rubisco activity (Vc,max) and increase in capacity for RuBP regeneration (Jmax) by (Bernacchi et al., 2005). Existing models of photosynthesis do not provide a means to link observed transcriptional changes with metabolism and photosynthetic capacity at the leaf level. Our integrated model overcomes this and not only suggests the changes in mRNA levels and how these affect photosynthetic metabolism, but was able to predict the acclimation of photosynthetic CO_2 assimilation that had been observed (Figure 1). Previous studies have reported proteome-level changes in response to elevated CO2 in soybean and other crop species (Ainsworth and Long, 2005, Bokhari et al., 2007, Taub et al., 2007, Yousuf et al., 2017, Zhao et al., 2019).

Interestingly, only 48 out of the 81 genes that encode enzymes in the e-Photosynthesis model had a statistically significant change in expression in elevated [CO_2], and only 17 had a fold change >1.5. Since the ratio of change in enzyme concentration was proportional to the change in transcript concentration, it reveals that even a slight modification to the e-Photosynthesis model resulted in better prediction accuracy of field observations. This result

462 represents the double-edged sword of multiscale modeling, in which fine-tuning at the molecular
463 level can have drastic consequences at higher scales. Errors can propagate in multiscale models
464 as information is exchanged across spatial and temporal scales. However, empirical validation of
465 the model outputs at any scale can minimize error propagation. In our study, field data
466 corroborated model simulations, providing confidence in the success of the modeling approach
467 and the biologically relevant flow of information from genes to organs.
468
469 *in silico perturbations identified transcriptional regulators of photosynthesis*
470 The successful manipulation of photosynthetic efficiency has been achieved through
471 targeted engineering of individual enzymes (Köhler et al., 2017, Driever et al., 2017), but an
472 alternative strategy is to simultaneously alter the expression of suites of enzymes involved in
473 different parts of the photosynthesis pathway (Simkin et al., 2017). Understanding the
474 transcriptional regulation of photosynthesis genes may help to fine-tune pathway expression
475 under different environmental conditions, so avoiding the need to directly engineer change in
476 expression of genes for each enzyme. This study uncovered three TFs, GmWRKY71,
477 GmGATA2, and a bHLH TF, which potentially regulate the expression of genes encoding key
478 enzymes involved in photosynthesis. While the transcriptional and post-transcriptional regulation
479 of genes involved in photosynthesis have previously been explored (Isono et al., 1997,
480 Fankhauser and Aubry, 2016, Saibo et al., 2008, Wang et al., 2017a, Zhang et al., 2016), this is
481 the first report of targeted GRN analysis to identify TFs that specifically co-regulate the
482 carboxylation of Rubisco and RubP regeneration.
483 Our hypothesis driven approach sought to explore how decreasing Rubisco and
484 reallocating resources to RubP regeneration might increase A_{sat}. The dynamic GRN identified
485 high-confidence TF-target gene relationships between photosynthesis genes that have a high
486 control coefficient and TFs tightly co-expressed with those genes. Using diverse training data,
487 we were able to derive weights associated with each TF-target interaction, indicating which TFs
488 exerted the greatest transcriptional control. Several TFs were found to co-regulate genes
489 affecting Rubisco and RubP regeneration (Figure 5). However, only GmGATA2 was predicted
490 to significantly down-regulate genes affecting Rubisco synthesis and up-regulating genes that
491 would increase RubP regeneration and starch synthesis. The multiscale model simulations for the
492 knockout and overexpression of GmGATA2 suggest a mechanism by which the transcriptional

493 regulation of key photosynthetic genes can alter flux through the pathway. For example, the
494 overexpression of GmGATA2 resulted in decreased V_{c_max} and increased J_{max}, as would be
495 required to maximize efficiency in an elevated [CO_2] environment (Table 2; (Drake et al., 1997,
496 Long et al., 2004)). The rewiring of metabolism, under both ambient and elevated CO_2, produces
497 a change in photosynthetic efficiency, which is a leaf-level phenotype. Specifically, the KO of
498 GmGATA2 decreases overall photosynthetic capacity only in ambient [CO2], while
499 overexpression results in a large decrease in carboxylation and increase in RubP regeneration
500 according to the A/Ci curve (Figure 6D).

501 All of the top candidate TFs from our model simulations belong to TF families that have
502 previously been implicated in the transcriptional regulation of photosynthesis (Saibo et al.,
503 2008). For example, bHLH TFs (Myc Family of TFs) were found to regulate aspects of C_4
504 photosynthesis that are also related to genes in the ancestral C_3 state (Borba et al., 2018).
505 Interestingly, a number of other studies identified the GATA family of transcription factors as
506 important regulators of photosynthesis and of carbon and nitrogen balance. The overexpression
507 of Class B GATAs and GLKs in Arabidopsis roots improved photosynthesis by increasing root
508 chlorophyll content (Ohnishi et al., 2018). GmGATA2 is annotated as NITRATE□INDUCIBLE,
509 CARBON METABOLISM□INVOLVED (GNC) and is homologous to AtGATA5, and both are
510 Class A GATAs that are associated with the light regulation of gene expression and
511 photomorphogenesis (Zhang et al., 2015). The overexpression of the poplar PdGNC gene in
512 Arabidopsis improved photosynthesis under low N levels by increasing the size and number of
513 chloroplasts per cell. The photosynthetic rate in transgenics increased by 42% compared to WT
514 lines (An et al., 2014). These studies with structurally or functionally similar GATA TFs provide
515 support for the role of GmGATA2 in the regulation of photosynthesis. Our GRN analysis
516 uncovered a strong positive correlation (co-expression) between GmGATA2 and FBP-aldolase
517 and starch synthase and a strong negative correlation (anti-correlation) between GmGATA2 and
518 the gene Rbcs that encodes the RuBisCO small sub-unit. Metabolic modeling and direct up-
519 regulation have suggested that both FBP-aldolase and starch synthase exert strong control on
520 RubP-regeneration (Zhu et al., 2007, Uematsu et al., 2012, Tian et al., 2018). These network
521 predictions provide testable hypotheses for the next round of experimentation and modeling.

522 The multiscale modeling strategy described here represents a uni-directional flow of
523 information from genes to physiological phenotype. However, bi-directional inputs and outputs

exist between the e-Photosynthesis model and the leaf micrometeorological model, in which the metabolic model can accept environmental parameters from the organ-level model. Ideally, a truly dynamic and biologically accurate model would have a bi- or multi-directional flow of information across scales. A limitation of this model is a lack of feedback from the metabolic model to gene expression. This limitation stems from an inadequate amount of species- and condition-specific transcriptional studies. Given the availability of more expression data, it would be possible to include a model component with switch-like behavior that pulls in appropriate expression data based on environment-level inputs. Alternatively, given protein expression data it may be possible to leverage the proportional relationship between change in protein concentration and change in transcript levels to predict gene expression based on protein levels. Regardless of the method, this gap in information flow is an area of focus to improve the current model. Moreover, this multiscale model is focused on one biological process, photosynthesis. The proof-of-concept modeling approach outlined in our study provides a feasible workflow, and a base model that can be expanded on to include related pathways and processes that are still black boxes and beyond the scope of in our current model.

Future directions.

We are now poised to explore the multiscale model generated hypotheses, including the functional testing of the top TF candidate genes. Ideally, these hypotheses will be tested directly in soybean through the generation of transgenic plants that can be grown in FACE experiments (Ainsworth et al., 2008). Likewise, the model is in place for expansion to include additional metabolic pathways, but also scale to other levels. For example, the leaf micrometeorological model is already a sub-component of a canopy-level model (Drewry et al., 2010, Srinivasan et al., 2017), so an intuitive next step would be link to models that provide 3-D biophysical representations of stands of plants, as for example those developed for sugarcane agronomy (Wang et al., 2017b). This allows simulations with more realistic inputs for light capture and competition between plants. Finally, advanced visualization of multiscale model outputs will be an important next step in the simulation and analysis of *in silico* crops. Combined modeling and visualization approaches will lead to realistic simulations of ideotypes to guide selection of genetic targets for crop improvement (Marshall-Colon et al., 2017).

555 *Conclusion*

556 Despite the many assumptions that have had to be made in this first linkage of gene expression
557 networks, through protein concentrations and photosynthetic metabolism to leaf level CO_2
558 exchange, it was successful in accurately predicting the observed acclimation of photosynthetic
559 capacity in soybean when grown under elevated [CO_2]. Most importantly it is shown to provide
560 a numerical means to identify from many hundreds of possible transcription factors, those most
561 likely to adapt photosynthetic efficiency to global atmospheric change. It opens the way to
562 guiding sustainable adaptation of crop photosynthesis to a range of both current and future
563 environments.

564

ACKNOWLEDGEMENTS

Funding for this work was provided by the FFAR, awards 515760 and 602757 to AMC, SPL, and MML and from a seed grant from the Institute for Sustainability, Energy, and Environment at UIUC, and the National Center for Supercomputing Applications at UIUC. The authors would like to thank Dr. Zoi Rapti and Dr. Saurabh Sinha at the University of Illinois for their guidance in development of the translation model and dynamic GRN, respectively. We thank Dr. Venkat Srinivasan, at the University of Illinois, for valuable discussions and advice on linking leaf energy balance with CO_2 assimilation and stomatal conductance.

Author Contributions: AMC, SPL, YW, and KK designed the study. KK, YW, GSC performed computational analysis. MML designed the computational interface. AMC, SPL, KK, YW, GSC, and MML wrote the paper.

REFERENCES

Ainsworth EA, Beier C, Calfapietra C, Ceulemans R, Durand-Tardif M, Farquhar GD, Godbold DL, Hendrey GR, Hickler T, Kaduk J, Karnosky DF, Kimball BA, Koerner C, Koornneef M, Lafarge T, Leakey ADB, Lewin KF, Long SP, Manderscheid R, McNeil DL, Mies TA, Miglietta F, Morgan JA, Nagy J, Norby RJ, Norton RM, Percy KE, Rogers A, Soussana JF, Stitt M, Weigel HJ, White JW. 2008. Next generation of elevated CO2 experiments with crops: a critical investment for feeding the future world. *Plant Cell and Environment,* **31**: 1317-1324.

Ainsworth EA, Long SP. 2005. What have we learned from 15 years of free-air CO2 enrichment (FACE)? A meta-analytic review of the responses of photosynthesis, canopy properties and plant production to rising CO2. *New phytologist,* **165**: 351-372.

Allocco DJ, Kohane IS, Butte AJ. 2004. Quantifying the relationship between co-expression, co-regulation and gene function. *BMC bioinformatics,* **5**: 18.

An Y, Han X, Tang S, Xia X, Yin W. 2014. Poplar GATA transcription factor PdGNC is capable of regulating chloroplast ultrastructure, photosynthesis, and vegetative growth in Arabidopsis under varying nitrogen levels. *Plant Cell, Tissue and Organ Culture (PCTOC),* **119**: 313-327.

Becskei A, Serrano L. 2000. Engineering stability in gene networks by autoregulation. *Nature,* **405**: 590.

Bernacchi CJ, Morgan PB, Ort DR, Long SP. 2005. The growth of soybean under free air [CO 2] enrichment (FACE) stimulates photosynthesis while decreasing in vivo Rubisco capacity. *Planta,* **220**: 434-446.

Bjorck A. 1996. *Numerical methods for least squares problems*: Siam.

Bokhari SA, Wan X-Y, Yang Y-W, Zhou L, Tang W-L, Liu J-Y. 2007. Proteomic response of rice seedling leaves to elevated CO2 levels. *Journal of proteome research,* **6**: 4624-4633.

Borba AR, Serra TS, Górska A, Gouveia P, Cordeiro AM, Reyna-Llorens I, Kneřová J, Barros PM, Abreu IA, Oliveira MM. 2018. Synergistic binding of bHLH transcription factors to the promoter of the maize NADP-ME gene used in C4 photosynthesis is based on an ancient code found in the ancestral C3 state. *Molecular biology and evolution,* **35**: 1690-1705.

Chew YH, Wenden B, Flis A, Mengin V, Taylor J, Davey CL, Tindal C, Thomas H, Ougham HJ, De Reffye P. 2014. Multiscale digital Arabidopsis predicts individual organ and whole-organism growth. *Proceedings of the National Academy of Sciences,* **111**: E4127-E4136.

Collatz GJ, Ball JT, Grivet C, Berry JA. 1991. Physiological and environmental regulation of stomatal conductance, photosynthesis and transpiration: a model that includes a laminar boundary layer. *Agricultural and Forest meteorology,* **54**: 107-136.

Drake BG, Gonzàlez-Meler MA, Long SP. 1997. More efficient plants: a consequence of rising atmospheric CO2? *Annual review of plant biology,* **48**: 609-639.

Drewry D, Kumar P, Long S, Bernacchi C, Liang XZ, Sivapalan M. 2010. Ecohydrological responses of dense canopies to environmental variability: 1. Interplay between vertical structure and photosynthetic pathway. *Journal of Geophysical Research: Biogeosciences,* **115**.

Driever SM, Simkin AJ, Alotaibi S, Fisk SJ, Madgwick PJ, Sparks CA, Jones HD, Lawson T, Parry MA, Raines CA. 2017. Increased SBPase activity improves photosynthesis and grain yield in wheat grown in greenhouse conditions. *Philosophical Transactions of the Royal Society B: Biological Sciences,* **372**: 20160384.

Edfors F, Danielsson F, Hallström BM, Käll L, Lundberg E, Pontén F, Forsström B, Uhlén M. 2016. Gene-specific correlation of RNA and protein levels in human cells and tissues. *Molecular systems biology,* **12**: 883.

El Samad H, Khammash M, Petzold L, Gillespie D. 2005. Stochastic modelling of gene regulatory networks. *International Journal of Robust and Nonlinear Control: IFAC□Affiliated Journal,* **15**: 691-711.

Fankhauser N, Aubry S. 2016. Post-transcriptional regulation of photosynthetic genes is a key driver of C4 leaf ontogeny. *Journal of experimental botany,* **68**: 137-146.

Farquhar GD, von Caemmerer Sv, Berry J. 1980. A biochemical model of photosynthetic CO 2 assimilation in leaves of C 3 species. *Planta,* **149**: 78-90.

Fell DA. 1998. Increasing the flux in metabolic pathways: a metabolic control analysis perspective. *Biotechnology and Bioengineering,* **58**: 121-124.

Higo K, Ugawa Y, Iwamoto M, Korenaga T. 1999. Plant cis-acting regulatory DNA elements (PLACE) database: 1999. *Nucleic acids research,* **27**: 297-300.

Isono K, Niwa Y, Satoh K, Kobayashi H. 1997. Evidence for transcriptional regulation of plastid photosynthesis genes in Arabidopsis thaliana roots. *Plant physiology,* **114**: 623-630.

Jin J, Zhang H, Kong L, Gao G, Luo J. 2013. PlantTFDB 3.0: a portal for the functional and evolutionary study of plant transcription factors. *Nucleic acids research,* **42**: D1182-D1187.

Karlebach G, Shamir R. 2008. Modelling and analysis of gene regulatory networks. *Nature Reviews Molecular Cell Biology,* **9**: 770.

Köhler L, Ebrahimizadeh Abrishami M, Roddatis V, Geppert J, Risch M. 2017. Mechanistic Parameters of Electrocatalytic Water Oxidation on LiMn2O4 in Comparison to Natural Photosynthesis. *ChemSusChem,* **10**: 4479-4490.

Lang M. 2019. yggdrasil: A Python Package for Integrating Computational Models Across Languages and Scales. *in silico Plants*.

Leakey AD, Xu F, Gillespie KM, McGrath JM, Ainsworth EA, Ort DR. 2009. Genomic basis for stimulated respiration by plants growing under elevated carbon dioxide. *Proceedings of the National Academy of Sciences*: pnas. 0810955106.

Li L, Nelson CJ, Trösch J, Castleden I, Huang S, Millar AH. 2017. Protein degradation rate in Arabidopsis thaliana leaf growth and development. *The Plant Cell,* **29**: 207-228.

Long SP, Ainsworth EA, Leakey AD, Nösberger J, Ort DR. 2006. Food for thought: lower-than-expected crop yield stimulation with rising CO2 concentrations. *science,* **312**: 1918-1921.

Long SP, Ainsworth EA, Rogers A, Ort DR. 2004. Rising atmospheric carbon dioxide: plants FACE the future. *Annu. Rev. Plant Biol.,* **55**: 591-628.

Marshall-Colon A, Long SP, Allen DK, Allen G, Beard DA, Benes B, von Caemmerer S, Christensen AJ, Cox DJ, Hart JC, Hirst PM, Kannan K, Katz DS, Lynch JP, Millar AJ, Panneerselvam B, Price ND, Prusinkiewicz P, Raila D, Shekar RG, Shrivastava S, Shukla D, Srinivasan V, Stitt M, Turk MJ, Voit EO, Wang Y, Yin XY,

669 **Zhu XG. 2017**. Crops In Silico: Generating Virtual Crops Using an Integrative and
670 Multi-scale Modeling Platform. *Frontiers in Plant Science,* **8**.
671 **Matys V, Kel-Margoulis OV, Fricke E, Liebich I, Land S, Barre-Dirrie A, Reuter I,**
672 **Chekmenev D, Krull M, Hornischer K. 2006**. TRANSFAC® and its module
673 TRANSCompel®: transcriptional gene regulation in eukaryotes. *Nucleic acids*
674 *research,* **34**: D108-D110.
675 **Medina-Rivera A, Defrance M, Sand O, Herrmann C, Castro-Mondragon JA, Delerce J,**
676 **Jaeger S, Blanchet C, Vincens P, Caron C. 2015**. RSAT 2015: regulatory sequence
677 analysis tools. *Nucleic acids research,* **43**: W50-W56.
678 **Millar AJ, Urquiza JU, Freeman PL, Hume A, Plotkin GD, Sorokina O, Zardilis A,**
679 **Zielinski T. 2019**. Practical steps to digital organism models, from laboratory
680 model species to 'Crops in silico. *Journal of experimental botany*.
681 **Nikolov NT, Massman WJ, Schoettle AW. 1995**. Coupling biochemical and biophysical
682 processes at the leaf level: an equilibrium photosynthesis model for leaves of C3
683 plants. *Ecological Modelling,* **80**: 205-235.
684 **Obayashi T, Kinoshita K. 2009**. Rank of correlation coefficient as a comparable measure
685 for biological significance of gene coexpression. *DNA research,* **16**: 249-260.
686 **Ohnishi A, Wada H, Kobayashi K. 2018**. Improved photosynthesis in Arabidopsis roots by
687 activation of GATA transcription factors. *Photosynthetica,* **56**: 433-444.
688 **Pachauri R, Meyer L, Plattner G, Stocker T. 2014**. IPCC, 2014: climate change 2014:
689 synthesis report. *IPCC, Geneva, Switzerland*.
690 **Raines CA. 2003**. The Calvin cycle revisited. *Photosynthesis research,* **75**: 1-10.
691 **Saibo NJ, Lourenço T, Oliveira MM. 2008**. Transcription factors and regulation of
692 photosynthetic and related metabolism under environmental stresses. *Annals of*
693 *botany,* **103**: 609-623.
694 **Sandelin A, Alkema W, Engström P, Wasserman WW, Lenhard B. 2004**. JASPAR: an
695 open-access database for eukaryotic transcription factor binding profiles. *Nucleic*
696 *acids research,* **32**: D91-D94.
697 **Shahmuradov IA, Gammerman AJ, Hancock JM, Bramley PM, Solovyev VV. 2003**.
698 PlantProm: a database of plant promoter sequences. *Nucleic acids research,* **31**: 114-
699 117.
700 **Simkin AJ, Lopez-Calcagno PE, Davey PA, Headland LR, Lawson T, Timm S, Bauwe H,**
701 **Raines CA. 2017**. Simultaneous stimulation of sedoheptulose 1,7-bisphosphatase,
702 fructose 1,6-bisphophate aldolase and the photorespiratory glycine decarboxylase-
703 H protein increases CO2 assimilation, vegetative biomass and seed yield in
704 Arabidopsis. *Plant Biotechnology Journal,* **15**: 805-816.
705 **Srinivasan V, Kumar P, Long SP. 2017**. Decreasing, not increasing, leaf area will raise
706 crop yields under global atmospheric change. *Global Change Biology,* **23**: 1626-1635.
707 **Stitt M, Sonnewald U. 1995**. Regulation of metabolism in transgenic plants. *Annual review*
708 *of plant biology,* **46**: 341-368.
709 **Taub D, MIller B, Allen H, Wang X. 2007**. OOS 30-4: Effects of elevated CO 2 on the
710 nutritional composition of food crops.
711 **Team RC. 2013**. R: A language and environment for statistical computing.
712 **Tian B, Talukder SK, Fu JM, Fritz AK, Trick HN. 2018**. Expression of a rice soluble starch
713 synthase gene in transgenic wheat improves the grain yield under heat stress
714 conditions. *In Vitro Cellular & Developmental Biology-Plant,* **54**: 216-227.

Uematsu K, Suzuki N, Iwamae T, Inui M, Yukawa H. 2012. Increased fructose 1,6-bisphosphate aldolase in plastids enhances growth and photosynthesis of tobacco plants. *Journal of Experimental Botany,* **63**: 3001-3009.

Von Caemmerer S. 2000. *Biochemical models of leaf photosynthesis*: Csiro publishing.

Walpole J, Papin JA, Peirce SM. 2013. Multiscale computational models of complex biological systems. *Annual review of biomedical engineering,* **15**: 137-154.

Wang P, Hendron RW, Kelly S. 2017a. Transcriptional control of photosynthetic capacity: conservation and divergence from Arabidopsis to rice. *New Phytologist,* **216**: 32-45.

Wang Y, Song QF, Jaiswal D, de Souza AP, Long SP, Zhu XG. 2017b. Development of a Three-Dimensional Ray-Tracing Model of Sugarcane Canopy Photosynthesis and Its Application in Assessing Impacts of Varied Row Spacing. *Bioenergy Research,* **10**: 626-634.

Weirauch MT, Yang A, Albu M, Cote AG, Montenegro-Montero A, Drewe P, Najafabadi HS, Lambert SA, Mann I, Cook K. 2014. Determination and inference of eukaryotic transcription factor sequence specificity. *Cell,* **158**: 1431-1443.

Woodrow IE. 1994. Optimal acclimation of the C 3 photosynthetic system under enhanced CO 2. *Photosynthesis Research,* **39**: 401-412.

Woodrow IE, Berry J. 1988. Enzymatic regulation of photosynthetic CO2, fixation in C3 plants. *Annual Review of Plant Physiology and Plant Molecular Biology,* **39**: 533-594.

Yousuf PY, Abd_Allah EF, Nauman M, Asif A, Hashem A, Alqarawi AA, Ahmad A. 2017. Responsive proteins in wheat cultivars with contrasting nitrogen efficiencies under the combined stress of high temperature and low nitrogen. *Genes,* **8**: 356.

Zhang C, Hou Y, Hao Q, Chen H, Chen L, Yuan S, Shan Z, Zhang X, Yang Z, Qiu D. 2015. Genome-wide survey of the soybean GATA transcription factor gene family and expression analysis under low nitrogen stress. *PloS one,* **10**: e0125174.

Zhang J, Du H, Chao M, Yin Z, Yang H, Li Y, Huang F, Yu D. 2016. Identification of two bZIP transcription factors interacting with the promoter of soybean rubisco activase gene (GmRCAα). *Frontiers in plant science,* **7**: 628.

Zhao X, Li W-F, Wang Y, Ma Z-H, Yang S-J, Zhou Q, Mao J, Chen B-H. 2019. Elevated CO 2 concentration promotes photosynthesis of grape (Vitis vinifera L. cv.'Pinot noir') plantlet in vitro by regulating RbcS and Rca revealed by proteomic and transcriptomic profiles. *BMC plant biology,* **19**: 42.

Zhu X-G, de Sturler E, Long SP. 2007. Optimizing the distribution of resources between enzymes of carbon metabolism can dramatically increase photosynthetic rate: a numerical simulation using an evolutionary algorithm. *Plant physiology,* **145**: 513-526.

Zhu X-G, Long SP, Ort DR. 2010. Improving photosynthetic efficiency for greater yield. *Annual review of plant biology,* **61**: 235-261.

Zhu XG, Wang Y, Ort DR, Long SP. 2013. e-photosynthesis: a comprehensive dynamic mechanistic model of C3 photosynthesis: from light capture to sucrose synthesis. *Plant, cell & environment,* **36**: 1711-1727.

TABLES

Table 1. The flux control coefficient of photosynthetic enzymes in ambient and elevated CO_2.

Enzyme	Value (μmol m-2 s-1)	Meta (AmbCO2)	Meta (EleCO2)	Meta+GE (EleCO2)	Meta+GE (EleCO2)*
Rubisco	120	0.443	0.121	0.165	0.108
Sedoheptulose-bisphosphatase	13.35	0.305	0.674	0.605	0.746
Fructose-bisphosphate aldolase	50.2	0.114	0.091	0.077	0.047
Glucose-1-phosphate adenylyltransferase	8.01	0.076	0.058	0.055	0.035
The maximum rate of ATP synthesis	6	0.054	0.047	0.081	0.051
Fructose-bisphosphatases	29.91	0.039	0.031	0.030	0.021
UTP-glucose-1-phosphate uridylyltransferase	3.46	0.021	0.014	0.014	0.009
Fructose-bisphosphatase (C)	1.92	0.014	0.010	0.011	0.007
Fructose-2,6-bisphosphate 2-phosphatase	0.5	0.010	0.007	0.006	0.004
Transketolase	128.57	0.008	0.003	0.003	0.001
Fructose-bisphosphate aldolase (C)	3.22	0.007	0.005	0.005	0.003
Glycine transaminase	82.37	0.007	0.002	0.001	0.001
(S)-2-hydroxy-acid oxidase &Catalase(CAT, EC1.11.1.6)	43.68	0.001	0.000	0.000	0.000
Sucrose-phosphate synthase	1.67	0.001	0.001	0.002	0.002
Phosphoribulokinase	446.19	0.001	-0.001	-0.001	0.000
glycine dehydrogenase (aminomethyl-transferring)	74.84	0.000	0.000	0.000	0.000
Glycerate kinase	171.47	-0.001	0.001	-0.001	0.000
Glyceraldehyde-3-phosphate dehydrogenase (NADP+)	166.35	-0.001	0.001	0.001	0.000
Glycerate dehydrogenase	300.29	-0.001	0.000	0.000	0.000
Phosphoglycolate phosphatase	1572.6	-0.001	0.000	0.000	0.000
Sucrose-phosphate phosphatase	16.65	-0.002	0.000	0.000	0.000
Serine-glyoxylate transaminase	99.19	-0.004	-0.003	-0.002	-0.001
6-phosphofructo-2-kinase	3.03	-0.009	-0.006	-0.006	-0.003
Fructose-bisphosphate aldolase	50.2	-0.015	-0.010	-0.008	-0.004
Phosphoglycerate kinase	1241.24	-0.030	-0.023	-0.023	-0.016
Photosynthesis rate		24.876	29.176	29.047	29.261

* Assuming the total nitrogen (protein) resource is a constant

Table 2. The V_{cmax} and J_{max} of the predicted ACi curves. The V_{cmax} and J_{max} were predicted using A/Ci curve fitting utility version 2.0 (Sharkey, 2015).

Treatment	V_{cmax}(25°C)	J_{max}(25°C)
WT-Amb	115.49	149.22
WT-Ele	109.17	152.57
WT-Ele (ConN)	112.29	153.58

bHLH TFOx-Amb	12.97	33.55
bHLH TFOx-Ele	110.66	90.71
bHLH TFKo-Amb	116.43	153.05
bHLH TFKo-Ele	114.54	154.51
GmWRKY71Ox-Amb	115.12	153.5
GmWRKY71Ox-Ele	112.08	154.97
GmWRKY71Ko-Amb	116.02	142.86
GmWRKY71Ko-Ele	113.37	151.82
bHLH TFKo&GmWRKY71Ox-Amb	118.93	154.76
bHLH TFKo&GmWRKY71Ox-Ele	114.67	155.78
GmGATA2Ox-Amb	91.28	157.58
GmGATA2Ox-Ele	89.67	157.59
GmGATA2Ko-Amb	123.28	135.62
GmGATA2Ko-Ele	119.75	147.49

ConN: Assuming the total nitrogen (protein) resource is a constant

FIGURE LEGENDS

Figure 1. Simulated and measured (Bernacchi et al., 2005) photosynthetic carbon dioxide response curves of soybean growing in ambient CO_2 (370 μmol mol^{-1}) and elevated CO_2 (550 μmol mol^{-1}). PAR is 2000 μmol m^{-2} s^{-1}

Figure 2. Model integration schematic describing the scaling from the gene regulatory network model to the metabolic model to the leaf physiological model. Note that these models interact through state variable indicated in the arrows. Ca is ambient CO_2 concentration, PPFD is the amount of light absorbed by the leaf, T is leaf temperature and A is the net carbon assimilation.

Figure 3. Metabolic model predicted metabolite concentrations without and with gene expression data (GE). PAR is 1200 μmol m^{-2} s^{-1}.

Figure 4. Gene expression level changes in target genes of interest as a result of *in silico* perturbation of three candidate TFs from the photosynthesis GRN. Figure shows mRNA expression levels in wild type and perturbed TF (bHLH TF knockout in a, GmWRKY71 overexpression in b, simultaneous knockout of bHLH TF and GmWRKY71 overexpression in c, GmGATA overexpression in d) conditions under ambient and elevated CO_2.

Figure 5. Gene regulatory network of metabolic genes having control coefficient > 0.01 based on sensitivity analysis of the metabolic model enzymes after incorporating gene expression data. Figure shows transcription factors as triangles and metabolic genes as squares. The network also shows change in mRNA expression of these genes under elevated CO_2 concentration in leaves with blue nodes indicating downregulation and orange nodes indicating upregulation under elevated CO_2 as compared to ambient CO_2. Similarly, blue edges indicate predicted repression and orange edges indicate predicted activation of the metabolic gene by the TF. Thickness of the edges are based on linear model weights with more thickness indicating a heavier weight associated with the TF-target interaction.

Figure 6. Predicted influence of transcription factor perturbations on photosynthesis rate a) bHLHB TF Knockout; b) GmWRKY71 Overexpression; c) bHLH TF Ko + GmWRKY71 Ox; d) GmGATA2 Overexpression.

SUPPLEMENTARY TABLES AND FIGURES

Supplemental figure 1. Simulated variation of assimilation (a), transpiration (b), stomatal conductance (c), and leaf temperature (d) as a function of leaf internal CO_2 concentration under ambient CO_2 (black) and elevated CO_2 (red). PPFD is 1200 µmol m^{-2} s^{-1}

Supplemental figure 2. Sub-networks for three transcription factors from the dynamic photosynthesis GRN chosen for *in silico* perturbation. The figure consists of bHLH TF (a), GmGATA2 (b) and GmWRKY71 (b) along with their predicted direct targets. Network nodes and interactions can be interpreted as in figure 5 of the main text.

Supplemental table 1. Least squares optimized weights for transcription factors regulating enzymes with high control coefficient after integration of protein translation model with e-photosynthesis metabolic model in the dynamic photosynthesis GRN. This table is provided separately as an excel workbook.

Supplemental table 2. Gene specific ‘d’ parameter values used in the protein translation model

Supplemental table 3. Vmax, Kcat, molecular weight and protein content used in the e-photosynthesis metabolic model

Supplemental table 4. Leaf level photosynthesis model parameters

812 Supplemental table 5. Steady state protein concentration ratios predicted by the protein
813 translation model for enzymes that are part of the e-photosynthesis model
814
815 **Appendix 1 Abbreviations and units – Some variables have been added here**
816 A: Net carbon assimilation (µmol m^{-2} s^{-1})
817 A_{sat}: Light saturated A (µmol m^{-2} s^{-1})
818 C_i: Leaf intercellular CO_2 concentration (µmol mol^{-1})
819 [CO_2]: Atmospheric CO_2 concentration (µmol mol^{-1})
820 FACE: Free Air [CO_2] Enrichment
821 g_s: Stomatal conductance (mmol m^{-2} s^{-1})
822 J: Rate of electron transport (µmol m^{-2} s^{-1})
823 J_{max}: Maximum rate of electron transport (µmol m^{-2} s^{-1})
824 R_d: Mitochondrial respiration (µmol m^{-2} s^{-1})
825 Rubisco: Ribulose-1,5-bisphosphate carboxylase/oxygenase
826 RubP: Ribulose-1,5-bisphosphate
827 SoyFACE: Soybean Free Air [CO_2] Enrichment
828 T_{leaf}: Leaf temperature (°C)
829 $V_{c,max}$: Maximum velocity of carboxylation (µmol m^{-2} s^{-1})
830
831
832
833

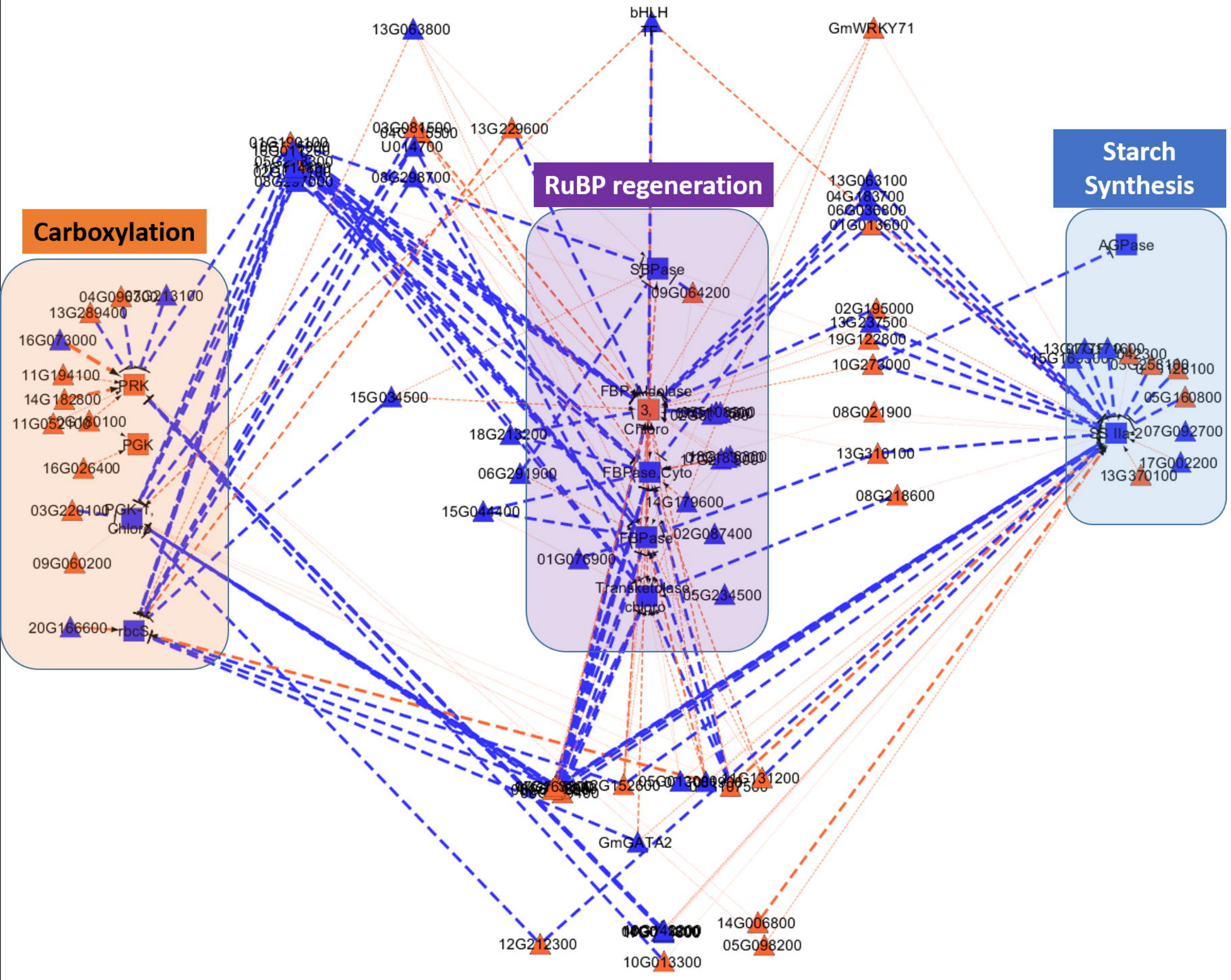
Carboxylation
RuBP regeneration
Starch Synthesis
bHLH TF
13G063800
GmWRKY71
13G229600
08G298700
SBPase
09G064200
FBP Aldolase 3, Chloro
FBPase Cyto
14G179600
FBPase
02G087400
01G076900
Transketolase chloro
05G234500
15G034500
18G213200
06G291900
15G044400
13G063100
04G183700
06G036800
01G013600
02G195000
13G237500
19G122800
10G273000
08G021900
13G310100
08G218600
AGPase
05G160800
17G002200
13G370100
13G289400
16G073000
11G194100
PRK
14G182800
PGK
16G026400
03G220100
PGK-T, Chloro
09G060200
20G166600
rbcS
GmGATA2
12G212300
10G013300
14G006800
05G098200

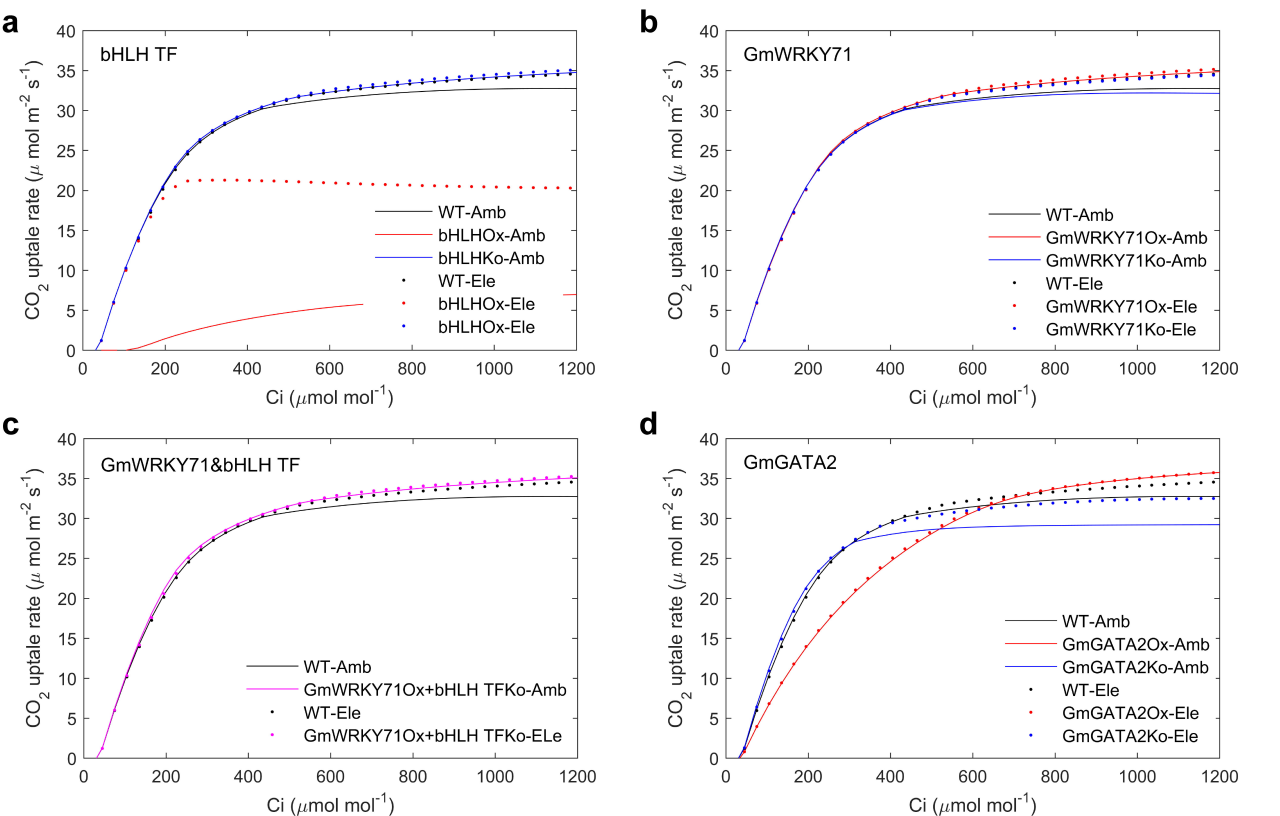
a
bHLH TF
WT-Amb
bHLHOx-Amb
bHLHKo-Amb
WT-Ele
bHLHOx-Ele
bHLHOx-Ele
b
GmWRKY71
WT-Amb
GmWRKY71Ox-Amb
GmWRKY71Ko-Amb
WT-Ele
GmWRKY71Ox-Ele
GmWRKY71Ko-Ele
c
GmWRKY71&bHLH TF
WT-Amb
GmWRKY71Ox+bHLH TFKo-Amb
WT-Ele
GmWRKY71Ox+bHLH TFKo-ELe
d
GmGATA2
WT-Amb
GmGATA2Ox-Amb
GmGATA2Ko-Amb
WT-Ele
GmGATA2Ox-Ele
GmGATA2Ko-Ele
CO2 uptale rate (μ mol m-2 s-1)
Ci (μmol mol-1)

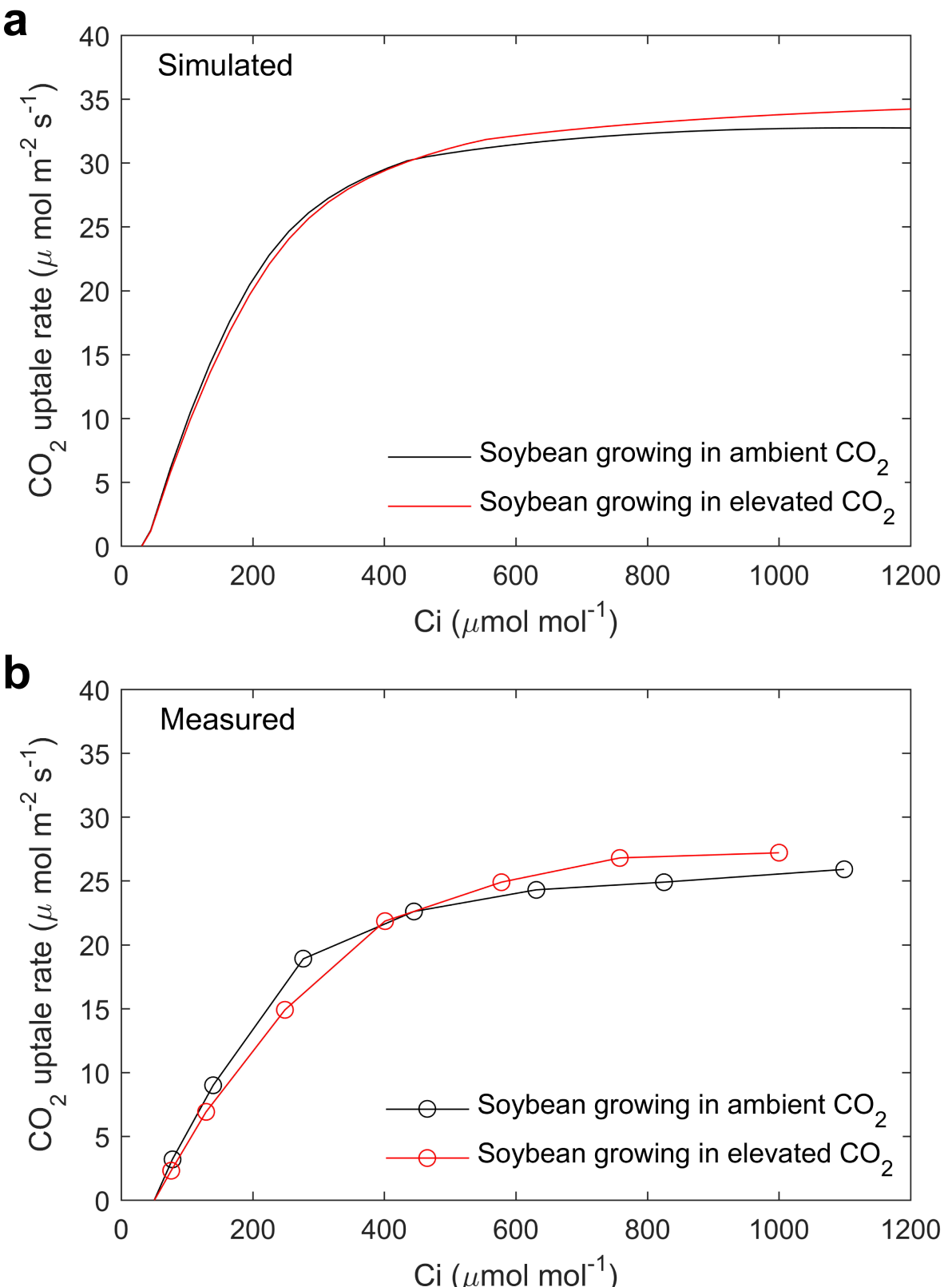
a
Simulated
CO_2 uptale rate (μ mol m^{-2} s^{-1})
Ci (μmol mol^{-1})
Soybean growing in ambient CO_2
Soybean growing in elevated CO_2
b
Measured
CO_2 uptale rate (μ mol m^{-2} s^{-1})
Ci (μmol mol^{-1})
Soybean growing in ambient CO_2
Soybean growing in elevated CO_2

a

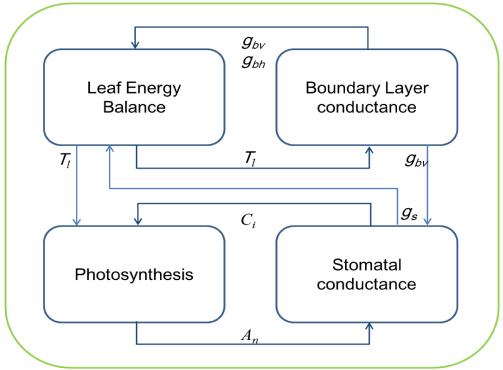

Photosynthesis rate

CO_2 concentration, light, temprature

CO_2 concentration

c

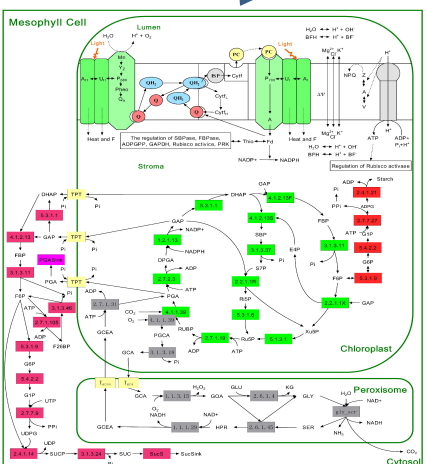

b

Protein concentration of enzymes

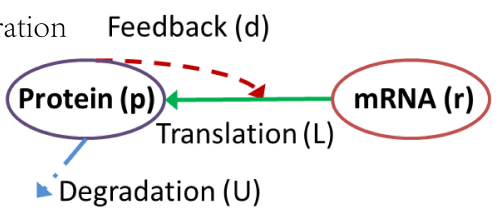

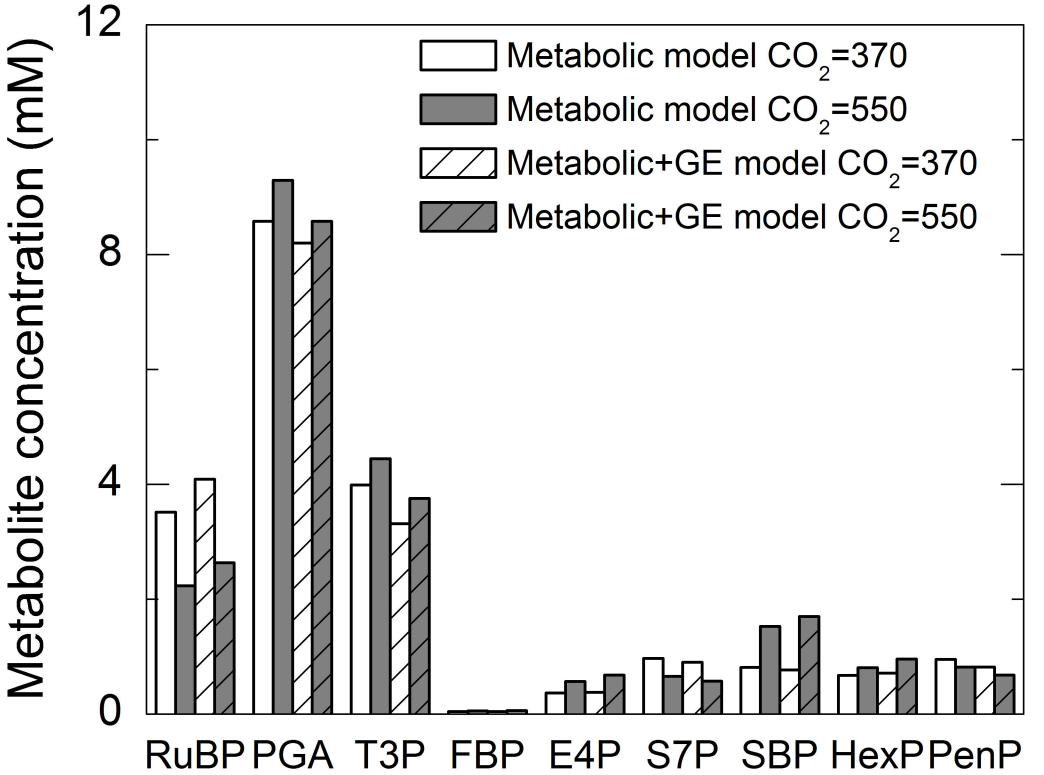
Metabolic concentration (mM)
12
8
4
0
Metabolic model CO2=370
Metabolic model CO2=550
Metabolic+GE model CO2=370
Metabolic+GE model CO2=550
RuBP
PGA
T3P
FBP
E4P
S7P
SBP
HexP
PenP

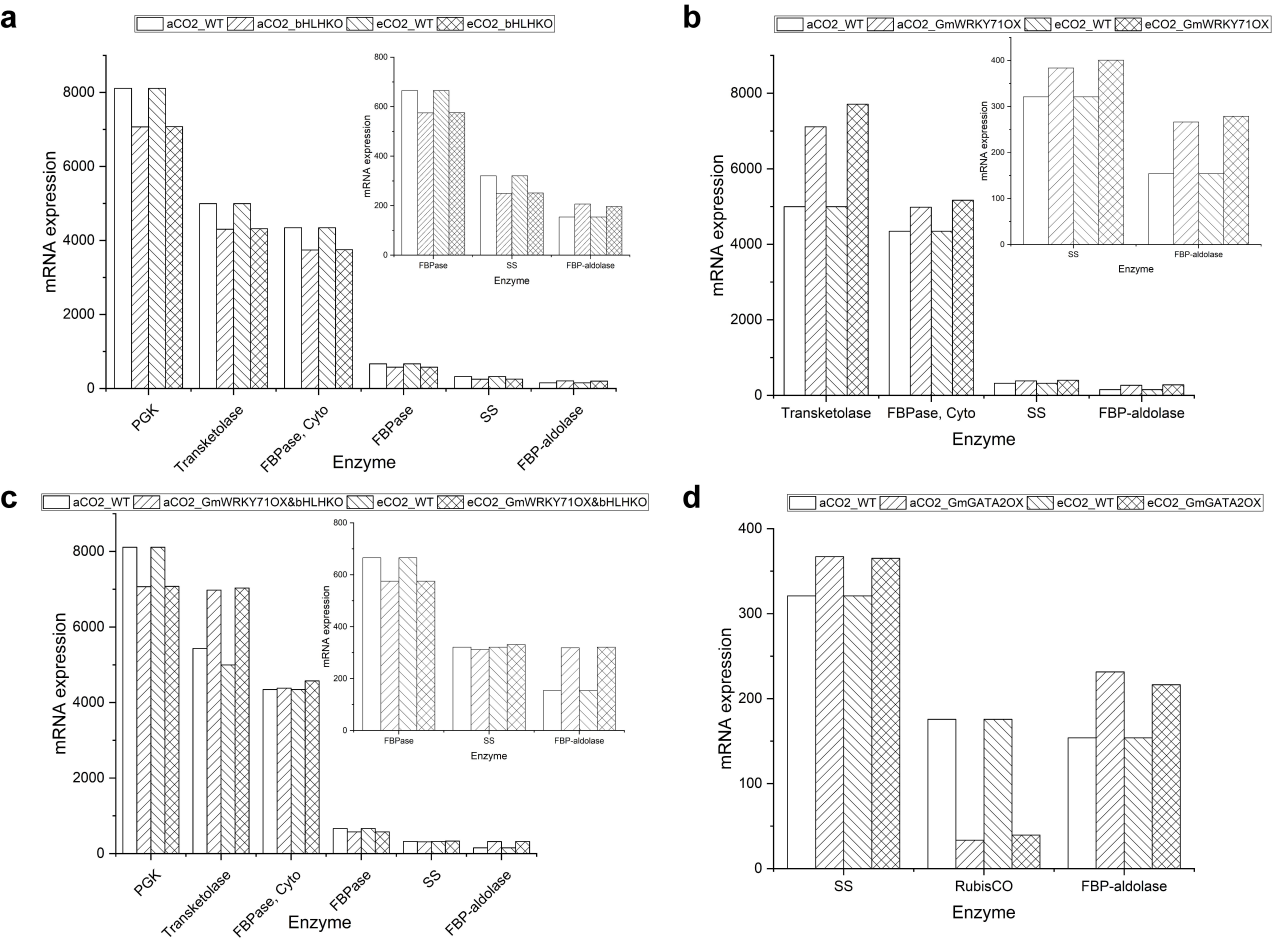
a
aCO2_WT
aCO2_bHLHKO
eCO2_WT
eCO2_bHLHKO
mRNA expression
8000
6000
4000
2000
0
PGK
Transketolase
FBPase, Cyto
FBPase
SS
FBP-aldolase
Enzyme
800
600
400
200
0
FBPase
SS
FBP-aldolase
Enzyme
b
aCO2_WT
aCO2_GmWRKY71OX
eCO2_WT
eCO2_GmWRKY71OX
mRNA expression
8000
6000
4000
2000
0
Transketolase
FBPase, Cyto
SS
FBP-aldolase
Enzyme
400
300
200
100
0
SS
FBP-aldolase
Enzyme
c
aCO2_WT
aCO2_GmWRKY71OX&bHLHKO
eCO2_WT
eCO2_GmWRKY71OX&bHLHKO
mRNA expression
8000
6000
4000
2000
0
PGK
Transketolase
FBPase, Cyto
FBPase
SS
FBP-aldolase
Enzyme
800
600
400
200
0
FBPase
SS
FBP-aldolase
Enzyme
d
aCO2_WT
aCO2_GmGATA2OX
eCO2_WT
eCO2_GmGATA2OX
mRNA expression
400
300
200
100
0
SS
RubisCO
FBP-aldolase
Enzyme